Ionic conductivity and the formation of cubic CaH2 in the LiBH4-Ca(BH4)2 composite

Sveinbjörnsson, Dadi Þorsteinn; Blanchard, Didier; Mýrdal, Jón Steinar Garðarsson; Younesi, Reza; Viskinde, Rasmus; Riktor, Marit Dalseth; Norby, Poul; Vegge, Tejs

Published in:
Journal of Solid State Chemistry

Link to article, DOI:
10.1016/j.jssc.2013.12.006

Publication date:
2014

www.elsevier.com/locate/jssc

Ionic Conductivity and the Formation of Cubic CaH_2 in the $LiBH_4$-$Ca(BH_4)_2$ Composite

Dadi Sveinbjörnsson, Didier Blanchard, Jon Steinar Gardarsson Myrdal, Reza Younesi, Rasmus Viskinde, Marit Dalseth Riktor, Poul Norby, Tejs Vegge

PII: S0022-4596(13)00593-8
DOI: http://dx.doi.org/10.1016/j.jssc.2013.12.006
Reference: YJSSC18292

To appear in: *Journal of Solid State Chemistry*

Received date: 8 October 2013
Revised date: 4 December 2013
Accepted date: 8 December 2013

Cite this article as: Dadi Sveinbjörnsson, Didier Blanchard, Jon Steinar Gardarsson Myrdal, Reza Younesi, Rasmus Viskinde, Marit Dalseth Riktor, Poul Norby, Tejs Vegge, Ionic Conductivity and the Formation of Cubic CaH_2 in the $LiBH_4$-$Ca(BH_4)_2$ Composite, *Journal of Solid State Chemistry*, http://dx.doi.org/10.1016/j.jssc.2013.12.006

Ionic Conductivity and the Formation of Cubic CaH_2 in the $LiBH_4$-$Ca(BH_4)_2$ Composite

Dadi Sveinbjörnsson[1], Didier Blanchard[1], Jon Steinar Gardarsson Myrdal[1,2], Reza Younesi[1], Rasmus Viskinde[1], Marit Dalseth Riktor[3], Poul Norby[1], Tejs Vegge[1,*].

[1]*Department of Energy Conversion and Storage, Technical University of Denmark, Frederiksborgvej 399, P.O. Box 49, DK-4000 Roskilde, Denmark.*
[2]*Center for Atomic-Scale Materials Design, Department of Physics, Technical University of Denmark, Anker Engelunds Vej 1, DK-2800 Lyngby, Denmark.*
[3]*Physics Department, Institute for Energy Technology, Instituttveien 18, P.O. Box 40, NO-2027 Kjeller, Norway.*

Abstract

$LiBH_4$-$Ca(BH_4)_2$ composites were prepared by ball milling. Their crystal structures and phase composition were investigated using synchrotron x-ray diffraction and Rietveld refinement, and their ionic conductivity was measured using impedance spectroscopy. The materials were found to form a physical mixture. The composites were composed of α-$Ca(BH_4)_2$, γ-$Ca(BH_4)_2$ and orthorhombic $LiBH_4$, and the relative phase quantities of the $Ca(BH_4)_2$ polymorphs varied significantly with $LiBH_4$ content. The formation of small amounts of orthorhombic CaH_2 and cubic CaH_2 in a CaF_2-like structure was observed upon heat treatment. Concurrent formation of elemental boron may also occur. The ionic conductivity of the composites was measured using impedance spectroscopy, and was found to be lower than that of ball milled $LiBH_4$. Electronic band structure calculations indicate that cubic CaH_2 with hydrogen defects is electronically conducting. Its formation along with the possible precipitation of boron therefore has an effect on the measured conductivity of the $LiBH_4$-$Ca(BH_4)_2$ composites and may increase the risk of an internal short-circuit in the cells.

Keywords

Lithium borohydride; Calcium borohydride; Calcium hydride; Solid electrolyte; Ionic conductivity; X-ray diffraction

* Corresponding author; phone: +45 46775810; fax: +45 46775688; e-mail: teve@dtu.dk.

Ionic Conductivity and the Formation of Cubic CaH_2 in the $LiBH_4$-$Ca(BH_4)_2$ Composite

Dadi Sveinbjörnsson[1], Didier Blanchard[1], Jon Steinar Gardarsson Myrdal[1,2], Reza Younesi[1], Rasmus Viskinde[1], Marit Dalseth Riktor[3], Poul Norby[1], Tejs Vegge[1,*].

[1]*Department of Energy Conversion and Storage, Technical University of Denmark, Frederiksborgvej 399, P.O. Box 49, DK-4000 Roskilde, Denmark.*
[2]*Center for Atomic-Scale Materials Design, Department of Physics, Technical University of Denmark, Anker Engelunds Vej 1, DK-2800 Lyngby, Denmark.*
[3]*Physics Department, Institute for Energy Technology, Instituttveien 18, P.O. Box 40, NO-2027 Kjeller, Norway.*

Abstract

$LiBH_4$-$Ca(BH_4)_2$ composites were prepared by ball milling. Their crystal structures and phase composition were investigated using synchrotron x-ray diffraction and Rietveld refinement, and their ionic conductivity was measured using impedance spectroscopy. The materials were found to form a physical mixture. The composites were composed of α-$Ca(BH_4)_2$, γ-$Ca(BH_4)_2$ and orthorhombic $LiBH_4$, and the relative phase quantities of the $Ca(BH_4)_2$ polymorphs varied significantly with $LiBH_4$ content. The formation of small amounts of orthorhombic CaH_2 and cubic CaH_2 in a CaF_2-like structure was observed upon heat treatment. Concurrent formation of elemental boron may also occur. The ionic conductivity of the composites was measured using impedance spectroscopy, and was found to be lower than that of ball milled $LiBH_4$. Electronic band structure calculations indicate that cubic CaH_2 with hydrogen defects is electronically conducting. Its formation along with the possible precipitation of boron therefore has an effect on the measured conductivity of the $LiBH_4$-$Ca(BH_4)_2$ composites and may increase the risk of an internal short-circuit in the cells.

Keywords

Lithium borohydride; Calcium borohydride; Calcium hydride; Solid electrolyte; Ionic conductivity; X-ray diffraction

1. Introduction

Research on lithium batteries is an important part of developing more sustainable and more efficient energy storage methods. Lithium batteries are dominant in the portable electronics sector today. However, for applications on a larger scale, such as in the transportation sector, substantial improvements are needed in terms of energy density, safety, charge-discharge cycle lifetime and price. Conventional Li-ion batteries use electrolytes made of organic liquids or gels. The main advantage of such electrolytes is their high Li^+ conductivity. They are, however, flammable and can cause safety issues. They can also allow for dendrite formation at the electrode-electrolyte interface, resulting in a decrease in cell capacity and a limited charge-discharge cycle life [1–3].

* Corresponding author; phone: +45 46775810; fax: +45 46775688; e-mail: teve@dtu.dk.

The usage of solid-state electrolytes, instead of the currently used liquids or gels, would increase the safety and should lead to an extended cycle life of the batteries. It is, however, challenging to develop solid electrolyte materials with sufficient chemical and electrochemical stability while offering high Li^+ conduction but negligible electronic conduction [4]. There are many currently known crystalline solid-state Li^+ conductors [2]. Among these are Li_3N [5], perovskite type oxides such as lithium lanthanum titanate (LLTO) [6–8], garnet type structures such as $Li_6BaLa_2Ta_2O_{12}$ [9], NASICON type structures [10,11], LISICON type structures [12] and $Li_{10}GeP_2S_{12}$ [13]. Most of these materials, however, have problems such as too low decomposition voltage (Li_3N), instability towards contact with elemental lithium (LLTO and NASICON) or too high electronic conductivity (LLTO) [14].

A Li^+ conductivity of 1 mS/cm is often cited as the minimum conductivity required for electrolytes to function well in consumer batteries [15,16]. For comparison 1 M $LiPF_6$ in EC-DMC (ethylene carbonate plus dimethyl carbonate), a widely used organic liquid electrolyte, has a Li^+ conductivity of 12 mS/cm at 27°C [17]. All above-mentioned crystalline solid electrolytes have considerably lower Li^+ conductivities, with the exception of $Li_{10}GeP_2S_{12}$ which has a Li^+ conductivity of 12 m/S/cm at 27°C [13].

Lithium borohydride has been investigated extensively in recent years, both as a hydrogen storage material [18–23] and as a crystalline solid electrolyte material for lithium batteries [24–26]. It is lightweight (0.666 g/cm^3) and has been shown to be electrochemically stable up to 5 V [27]. At room temperature, $LiBH_4$ has an orthorhombic crystal structure (*Pnma*) with a low Li^+ conduction (approx. 10^{-8} S/cm at 30°C), but undergoes a reversible phase transition at around 110°C to a hexagonal crystal structure ($P6_3m_c$) with a high Li^+ conduction (approx. 10^{-3} S/cm at 120°C) [24,28]. The hexagonal structure can be stabilized at room temperature by adding lithium halides (LiI, LiBr and LiCl) [29,30]. Such addition has been found to result in an even higher Li^+ conductivity than seen in hexagonal $LiBH_4$. Studies on the structural and Li^+ conduction properties of the $LiBH_4$-LiI solid solution have recently been published [31–34].

Calcium borohydride has also been investigated extensively as a hydrogen storage material [35–42]. The crystal structures of $Ca(BH_4)_2$ were only resolved relatively recently, and four polymorphs of calcium borohydride have been characterized. α-$Ca(BH_4)_2$ has an orthorhombic structure (*Fddd* [35] or *F2dd* [43]). β- $Ca(BH_4)_2$ has a tetragonal crystal structure (*P- 4*[43] or $P4_2/m$ [44]). β- $Ca(BH_4)_2$ is sometimes referred to as a high-temperature polymorph, as it has been observed to become the dominant phase above 130°C [44]. γ-$Ca(BH_4)_2$ has an orthorhombic crystal structure (*Pbca*) [45]. The fourth polymorph, α'-$Ca(BH_4)_2$, is a high-temperature modification of the α structure that appears by a second order phase transition at around 220°C. This polymorph has a tetragonal crystal structure (*I-42d*, a supergroup of *F2dd*) [43] and was not observed in this work.

As the enthalpy differences between the α, β, and γ polymorphs are rather small (35-135 meV) [45,46], these usually coexist. The relative quantity of the phases can even differ significantly between batches [42]. As shown in this work, the addition of $LiBH_4$ possibly has a large effect on the relative quantities of the $Ca(BH_4)_2$ polymorphs, which depend heavily on the mixing ratio of the two compounds. Furthermore, the possibility of Ca^{+2} substitution in $LiBH_4$ is discussed in this work, as such introduction of relatively large cations in $LiBH_4$ could lead to compensating vacancies, which would likely enhance the Li^+ conduction. As an example, divalent doping of chlorides has been found to increase their ionic conductivity [47].

Reports on the structure and hydrogen storage properties of the $LiBH_4$-$Ca(BH_4)_2$ composite have been published [48,49]. Accounts of the nature of the $LiBH_4$-$Ca(BH_4)_2$ mixtures differ, however, as Z. Fang et al. reported on the formation of a dual-cation borohydride $LiCa(BH_4)_3$, while J. Y. Lee et al. concluded that $LiBH_4$ and $Ca(BH_4)_2$ coexist as a physical mixture but not as a compound or a solid solution. We shall seek to resolve this controversy by reporting on the structural properties of the $LiBH_4$-$Ca(BH_4)_2$ mixtures using synchrotron x-ray diffraction. In the present work we report on the crystal structures and the phase composition of $(1-x)LiBH_4+xCa(BH_4)_2$ mixtures in various ratios. The main focus of the work is on the ionic conductivity of the composites and on the formation of CaH_2 in both

orthorhombic and cubic structures that was observed upon heat treatment of the $LiBH_4$-$Ca(BH_4)_2$ composites. Furthermore, we will discuss how the low chemical stability of $LiBH_4$-$Ca(BH_4)_2$, illustrated by the formation of CaH_2, affects the suitability of the mixtures for usage as solid electrolytes, and how this can increase the risk of a short-circuit in the cell.

2. Experimental and Computational Methods

2.1 Preparation of the Composites

$LiBH_4$ powder (purity 95%) and $Ca(BH_4)_2$ were purchased from Alfa Aesar Co. and Sigma Aldrich Co. respectively. The $(1-x)LiBH_4+xCa(BH_4)_2$ samples were prepared in nine different ratios, with $x = \{0, 0.125, 0.1875\ 0.25, 0.33, 0.5, 0.67, 0.75, 1.0\}$. The mixing was performed by planetary ball milling under Ar atmosphere. In each milling, a stainless steel vial with an inner volume of 250 ml was rotated at 650 rpm for 2 hours on a Fritsch Pulverisette P6. 1.0, 1.5 or 2.0 g of precursor powder were inserted into the vial for each milling along with 25 tungsten carbide balls, resulting in a sample to balls mass ratios of 1/400, 1/300 or 1/200 respectively.

2.2 Powder X-ray Diffraction (XRD)

The samples were characterized using powder x-ray diffraction (XRD). The measurements were performed on the as-milled samples. The diffraction patterns used in this work were obtained at three different instruments.

The diffraction patterns of the $(1-x)LiBH_4+xCa(BH_4)_2$ samples with $x = \{0.125, 1.0\}$ were measured at the BM01A beam line of the Swiss-Norwegian Beamlines (SNBL) located at the European Synchrotron Radiation Facility (ESRF) in Grenoble, France. The samples were mounted in glass capillaries sealed under Ar atmosphere using an epoxy adhesive. The two-dimensional diffraction data were collected at the Pilatus@SNBL diffractometer, using a Pilates 2M detector, with a distance of 310 mm between the sample and the detector. The wavelength was 0.69386 Å. Data processing was carried out using the SNBL Tool Box [50]. The two-dimensional data were calibrated with a NIST LaB_6 standard sample.

The diffraction patterns of the samples with $x = \{0.25, 0.5\}$ were measured at the beamline I11 located at the Diamond Light Source in Oxfordshire, England. The sample mounting was the same as described above. A Mythen II PSD detector was used at 2θ angles ranging from 1° to 91°. The wavelength was 0.82712 Å. The data were calibrated using Si as an external standard.

The diffraction patterns of the samples with $x = \{0, .1875, 0.33, 0.67, 0.75\}$ were measured using a Cu K_α Bruker D8 diffractometer with a Bragg-Brentano geometry, operating at 40 kV and 40 mA. The samples were sealed under Ar atmosphere in an airtight polyethylene sample holder from Bruker Co. The exposure time was 3 s/step with a step size of 0.02°. The measurements were performed using a variable divergence slit. After the measurement, the intensity of the data was corrected for the variable slit size and the $K_{\alpha 2}$ signal was subtracted. All XRD measurements were performed at room temperature. The synchrotron data were integrated into one-dimensional powder diffraction patterns using the Fit2D software [51].

For all diffraction patterns, Rietveld refinement was carried out using the GSAS software [52]. The phase factors, the unit cell parameters as well as the strain and the size broadening parameters were refined for all phases. Pseudo-Voigt profiles were used for modeling the shapes of the diffraction peaks. The background signal was modeled using a polynomial expression, and the zero point was refined. The isotropic thermal motion parameters were refined for all atoms except hydrogen and preferred diffraction orientations in the powder were modeled if needed. The occupancy of Ca^{+2} was refined in α-$Ca(BH_4)_2$ and the γ-$Ca(BH_4)_2$ phases. The resulting values for γ-$Ca(BH_4)_2$ are shown in Table 1. For α-$Ca(BH_4)_2$ the refinement of the Ca^{+2} positions showed full occupancies. The peak to parameter ratio was greater than 2 for all refinements and greater than 5 for most refinements. The weighted

profile agreement factor R_{wp} at the end of the refinements ranged from 2.2% to 4.25% and the data were refined for convergence, i.e. until the squared sum of all parameter shifts divided by the estimated standard deviation (i.e. $\Sigma(\text{shift}/\sigma)^2$) reached < 0.1.

2.3 Impedance Spectroscopy (EIS)

The conductivities of the samples were measured by AC impedance spectroscopy using a PARSTAT 2273 potentiostat. The ball-milled powder was pressed into pellets with a diameter of 13 mm and a thickness of approx. 2 mm. Lithium foil was pressed onto both faces of the pellets as electrodes. The powder and the lithium foil were pressed simultaneously at 1 ton/cm^2. The porosity of the pellets was found to be around 0.4. All preparation and measurements were carried out under Ar atmosphere. The frequency range of the impedance measurements was set from 100 mHz to 1 MHz. The samples were heated up from 30°C to 100°C in steps of 5°C and cooled down to 30°C using the same step size. The samples were equilibrated at a constant temperature for at least 40 minutes prior to each measurement.

2.4 Energy-Dispersive X-ray Spectroscopy (EDS)

A Hitachi TM3000 scanning electron microscope (SEM) operating at 15 kV was used for performing EDS on a $0.875LiBH_4+0.125Ca(BH_4)_2$ sample after heat treating it up to a temperature of 100°C during the impedance spectroscopy measurements. The EDS samples were prepared by applying a thin layer of powder on carbon tape. The samples were transferred to the SEM instrument under Ar atmosphere. Elemental mapping was performed after each area scan or line scan of the sample.

2.5 X-ray Photoelectron Spectroscopy (XPS)

XPS measurements were performed on a $0.875LiBH_4+0.125Ca(BH_4)_2$ sample after heat treating it up to a temperature of 100°C during the impedance spectroscopy measurements. A PHI 5500 spectrometer was used, with monochromatic Al K_α radiation (1487 eV) and an electron emission angle of 45°. All the XPS spectra were energy calibrated by the hydrocarbon peak positioned at the binding energy of 285.0 eV. The XPS samples were prepared by applying a thin layer of powders on copper tape. The samples were transferred from a glove box to the XPS analysis chamber using a specially built airtight argon-filled chamber to avoid contamination from the air.

2.6 Electronic Structure Calculations

All electronic structure calculations presented in this work were performed using density functional theory (DFT) [53,54] as it is implemented in the GPAW code [55,56], using the atomic simulation environment (ASE) [57]. GPAW is based on real space grids and uses the projector-augmented wave method (PAW) to describe non-valence electrons [58,59]. All atomic structural relaxations were calculated using the PBE exchange and correlation functional [60] with a 0.15 Å grid spacing and a (4,4,4) k-point mesh. Each calculation was continued until all forces were below 0.01 eV/Å. Calculations of charged vacancy defects were performed with an extra electron in the computational supercell. The extra electron was treated exactly like all other electrons in the DFT calculations, but to prevent an infinite charge build-up over the periodic images of the cell, an equal opposite charge was smeared uniformly over the cell. Because of the uniform distribution of the compensation charge, its effect on the chemistry of the cell is negligible. Band gap calculations were performed using the GLLB-sc exchange and correlation functional [61], which has been shown to improve band gap description significantly from standard GGA functionals [62].

3. Results and Discussion

3.1 Crystal Structure and Phase Composition

The diffraction patterns of pure $LiBH_4$, pure $Ca(BH_4)_2$ and four composites of the two compounds are shown in Figure 1, along with a Rietveld refinement of each diffraction pattern. The diffraction pattern presented for $LiBH_4$ is from a ball-milled sample. For $Ca(BH_4)_2$, diffraction patterns were acquired for as-received and ball milled powders. We present only the diffraction pattern of the as-received compound since the milling alters the crystallinity of the powder, reducing the quality of the diffraction pattern and the Bragg peak intensities of the already poorly scattering $Ca(BH_4)_2$ powder. It was thus not possible to perform a trustworthy Rietveld refinement of the milled $Ca(BH_4)_2$.

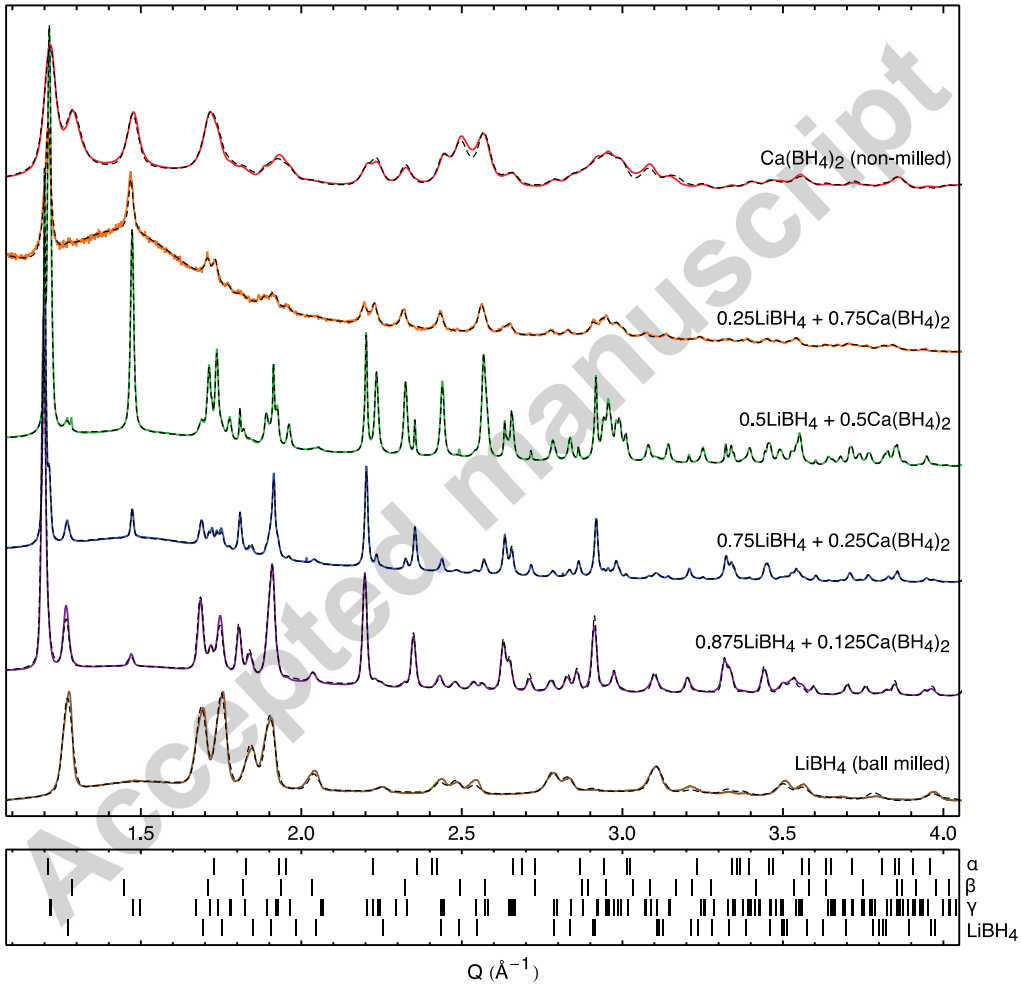

Figure 1 Powder x-ray diffraction patterns for different ratios of $(1\text{-}x)LiBH_4+xCa(BH_4)_2$. The solid, colored lines show the measured data, the dashed, black lines show the Rietveld refinement of each measurement. The tick marks below the diffraction patterns show the locations of the Bragg reflections of α-$Ca(BH_4)_2$, β-$Ca(BH_4)_2$ γ-$Ca(BH_4)_2$ and orthorhombic $LiBH_4$. No other phases were detected in the samples. The diffraction pattern of pure $LiBH_4$ only contains orthorhombic $LiBH_4$. In the diffraction pattern of pure $Ca(BH_4)_2$, β-$Ca(BH_4)_2$ and γ-$Ca(BH_4)_2$ coexist, but no α-$Ca(BH_4)_2$ is detected. In the $(1\text{-}x)LiBH_4+xCa(BH_4)_2$ mixtures, α-$Ca(BH_4)_2$, γ-$Ca(BH_4)_2$ and orthorhombic $LiBH_4$ coexist, but no β-$Ca(BH_4)_2$ is detected. All data in the figure comes from synchrotron measurements except for the sample with $x = 0.75$

Table 1 The relative phase quantities (in weight percentage) in the (1-*x*)$LiBH_4$+*x*$Ca(BH_4)_2$ samples, obtained from the Rietveld refinement of the XRD data. There are large variations in the phase quantities of the α and γ phases of $Ca(BH_4)_2$ with $LiBH_4$ content, but the β phase is only present in pure $Ca(BH_4)_2$. The phase quantity of orthorhombic $LiBH_4$ is expected to equal the actual $LiBH_4$ weight percentage in each sample. This means that, for an optimal refinement, the values of the fifth column of the table are expected to approach those in the sixth column. The Rietveld refinements are, however, somewhat imperfect with regard to this, most probably due to the low scattering power of $LiBH_4$ relative to $Ca(BH_4)_2$. The rightmost column of the table shows the refined Ca^{+2} occupancies in the α-$Ca(BH_4)_2$ phase, but only for those mixtures for which synchrotron data were available. The Ca^{+2} occupancies in the β-$Ca(BH_4)_2$ and γ-$Ca(BH_4)_2$ phases were found to be 1.0 in all diffractograms.

Sample (x in mol)	*α-$Ca(BH_4)_2$ (wt%)*	*β-$Ca(BH_4)_2$ (wt%)*	*γ-$Ca(BH_4)_2$ (wt%)*	*$LiBH_4$ LT (wt%)*	*Actual $LiBH_4$ wt% in sample*	*Ca^{+2} occupancy in α-$Ca(BH_4)_2$*
0.0	0.0	0.0	0.0	100.0	100.00	N/A
0.125	24.1	0.0	3.2	72.7	68.61	0.972
0.1875	22.1	0.0	13.2	64.7	57.50	N/A
0.25	39.0	0.0	10.6	50.4	48.37	0.931
0.33	6.2	0.0	46.5	47.3	38.50	N/A
0.50	8.7	0.0	62.4	28.9	23.80	0.975
0.67	18.0	0.0	65.0	17.0	12.97	N/A
0.75	15.8	0.0	62.7	21.5	9.43	N/A
1.00	0.0	36.9	63.1	0.0	0.00	N/A

The relative phase quantities of the mixtures in weight percentage, as obtained by Rietveld refinement, are shown in Table 1. The milled $LiBH_4$ sample only contains orthorhombic $LiBH_4$, as expected. The pure, as-received $Ca(BH_4)_2$ sample contains β-$Ca(BH_4)_2$ and γ-$Ca(BH_4)_2$, but no α-$Ca(BH_4)_2$ is present. All composites are composed of orthorhombic $LiBH_4$, α-$Ca(BH_4)_2$ and γ-$Ca(BH_4)_2$ only; no other phases or new compounds are formed during the ball milling. Note that the amount of $LiBH_4$ in the composite samples is generally overestimated compared to the actual mixing ratios of the samples. This indicates the accuracy of the Rietveld refinements performed on $LiBH_4$, which is composed of elements with low electron densities and is thus a poor x-ray scatterer relative to $Ca(BH_4)_2$. Small sample inhomogeneities may also contribute to the discrepancy in the $LiBH_4$ phase quantities.

As mentioned in the introduction, the enthalpy differences between the different $Ca(BH_4)_2$ phases are small, and therefore the relative phase quantities of the $Ca(BH_4)_2$ polymorphs are very sensitive to modifications of the mixture. Interestingly, no β-$Ca(BH_4)_2$ is detected in the composites although it is present in pure $Ca(BH_4)_2$. This is consistent with the findings of Lee *et al.* [48]. The relative quantities of the two remaining $Ca(BH_4)_2$ phases are very sensitive to any modifications of the mixture. α-$Ca(BH_4)_2$ is found to have the largest relative phase quantity for $x = 0.25$. For samples with large amounts of $LiBH_4$, only small amounts of γ-$Ca(BH_4)_2$ are found, but for composites with $x \geq 0.5$ it becomes the dominant phase with a similar relative phase quantity as in the pure $Ca(BH_4)_2$ sample.

The formation of α-$Ca(BH_4)_2$, which is not present in the as-received $Ca(BH_4)_2$, is either facilitated by the introduction of $LiBH_4$ (even in small amounts), or simply by the ball milling process. As already mentioned, the crystallinity of the pure, ball-milled $Ca(BH_4)_2$ samples was very poor, and it was unfortunately not possible to deduce the relative quantities of the $Ca(BH_4)_2$ polymorphs from the diffraction pattern. It can thus not be inferred with certainty whether the polymorph changes in $Ca(BH_4)_2$ take place due to $LiBH_4$ addition or due to the milling itself. It is, however, clear that the introduction of $LiBH_4$ increases the crystallinity of the $Ca(BH_4)_2$ polymorphs, as compared to the as-received and ball-milled $Ca(BH_4)_2$ samples.

The lattice parameters in all samples were found to deviate by less than 1% from those previously published for orthorhombic LiBH4 [28], α-$Ca(BH_4)_2$ [35], β-$Ca(BH_4)_2$ [44] and γ-$Ca(BH_4)_2$ [45]. The lattice parameters of the composite samples are in all cases very similar to those of the phases in the precursor compounds and do not change much with the mixing ratio *x*. We therefore conclude that the (1-*x*)$LiBH_4$+*x*$Ca(BH_4)_2$ composites are physical mixtures

rather than solid solutions. This finding is in good agreement with those previously reported by Lee et al [48].

After ball milling, a fraction of each sample was annealed in a glass container at 100°C for 60 hours under Ar atmosphere. XRD measurements of the annealed powders show that such heat treatment does not change the phase compositions, which remain very close to those presented in Table 1. It was therefore not expected that the heat treatment during the impedance spectroscopy measurements would alter the phase composition of the samples.

3.2 CaH_2 Formation

When the samples were heated up to 100°C during the impedance spectroscopy measurements (under Ar atmosphere), a new phase formed over the course of a few hours. This phase consisted of a black layer, growing at the interfaces between the Li electrodes and the electrolyte. This surprising finding was observed even if no potential was applied to the sample. In order to identify this phase, synchrotron XRD was performed on a black colored part of a sample. The resulting diffraction pattern is shown in Figure 2, along with a Rietveld refinement of the data. The majority of the powder consists of α-$Ca(BH_4)_2$ and orthorhombic $LiBH_4$. However, the data refinement reveals two additional phases that were not detected in the diffraction patterns of the as-milled samples shown in Figure 1. One of the phases was identified as CaH_2 in its regular orthorhombic (*Pnma*) crystal structure (3.6 wt%). The second phase was indexed as a cubic structure with the space group *Fm-3m*, isostructural with CaF_2. Its lattice parameter is 5.490 Å, compared to 5.4 Å for CaF_2. After further investigations, this cubic phase was identified as CaH_2 (4.2 wt%). The crystal structures and the lattice parameters of the detected phases in the diffraction pattern in Figure 2 are shown in Table 2. No other phases or unexplained Bragg peaks were detected in the diffraction pattern. That does, however, not fully exclude the presence of small amounts of poorly scattering phases such as elemental boron or lithium.

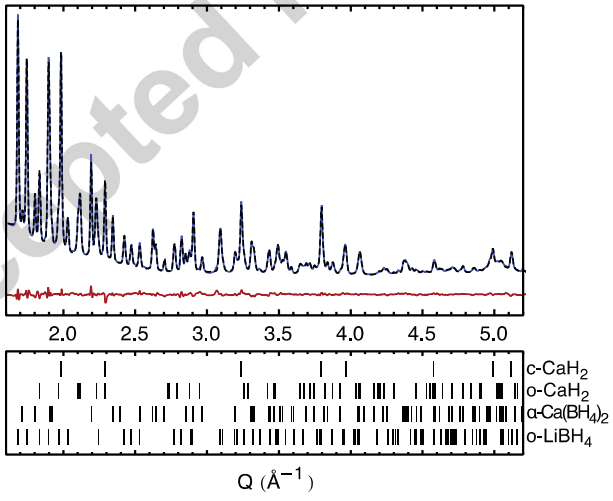

Figure 2 Synchrotron XRD data (from SNBL) and a Rietveld refinement of a black-colored part of a $0.875LiBH_4+0.125Ca(BH_4)_2$ sample after it had been heat treated up to a temperature of 100°C during the impedance spectroscopy measurements. The blue, solid line shows the measured data, the black, dashed line shows the Rietveld refinement of the data and the red, solid line on the bottom shows the difference between the measured data and the refinement. The Rietveld refinement reveals that the diffraction pattern consists of α-$Ca(BH_4)_2$, and orthorhombic $LiBH_4$, along with 3.6 wt% of orthorhombic CaH_2 and 4.2 wt% of cubic CaH_2 (in a CaF_2 crystal structure). No other phases were detected. The tick marks below the diffraction patterns show the locations of the diffraction peaks for the four phases according to the Rietveld refinement.

Table 2 The crystal structures and the lattice parameters of the refined structures in Figure 2.

Phase	*Crystal structure*	*a* (Å)	*b* (Å)	*c* (Å)
o-LiBH4	*Pnma*	7.201	4.452	6.857
α-$Ca(BH_4)_2$	*F2ddd*	8.815	13.184	7.543
o-CaH_2	*Pnma*	5.974	3.617	6.849
c-CaH_2	*Fm-3m*	5.488	5.488	5.488

Solid solutions of $CaH_{2-x}F_x$ in the cubic CaF_2 crystal structure with various concentrations of hydrogen have previously been reported, first by Brice et al. [63] and more recently in connection with research on $Ca(BH_4)_2$ thermal decomposition [64,65]. Smithson et al. [66] have performed *ab-initio* calculations that show that at zero pressure, the formation energies for orthorhombic CaH_2 and cubic CaH_2 are very similar. Pinatel et al. [67] have recently calculated the phase diagram of the $CaH_{2-x}F_x$ solid solution and found that the cubic and orthorhombic phases can coexist near room temperature with very a low concentration of fluoride. Furthermore, Li et al. have detected a high-pressure phase of CaH_2 using *in-situ* Raman scattering, which reportedly starts forming at about 15.5 GPa and is thought to possess a higher symmetry than orthorhombic CaH_2 [68].

To investigate the possibility of the formation of cubic CaH_2 without any fluoride content, the relative stability of the orthorhombic and the cubic CaH_2 phases was calculated. The calculations were performed for structures with and without a 1/8 density of hydrogen vacancies. The charge state of the vacancies is likely to be heavily dependent on the potential over the CaH_2. Therefore, the calculations were performed both for neutral vacancies and for vacancies with a single negative elementary charge. For the structures with no vacancies, orthorhombic CaH_2 is found to be more stable than cubic CaH_2 by 0.23 eV. However, when the hydrogen vacancies are introduced, cubic CaH_2 is found to be more stable than orthorhombic CaH_2 by 0.02 eV for neutral vacancies and 0.34 eV for charged vacancies. This indicates that for structures with crystal defects, cubic CaH_2 could form and probably coexist with orthorhombic CaH_2.The relative stability of the two phases in the case of no defects and in the case of charged vacancies are shown in Figure 3.

Note that the particular density of vacancies used for the calculations was simply chosen as a representative number and is not based on experimental findings. The main goal of the calculations was to see if the presence of vacancies would increase the stability of the orthorhombic phase relative to the cubic phase. The actual density of defects in the structure, if any, cannot be determined using the experimental techniques presented here, but could be measured using neutron diffraction as a part of further studies on this subject.

Figure 3 The calculated stability of cubic CaH_2 relative to orthorhombic CaH_2 for structures with no defects and for structures with a 1/8 (12.5%) density of charged hydrogen vacancies. The cubic structure is found to be more stable than the orthorhombic structure with the introduction of the H vacancies.

In the light of these results, we consider it very likely that the local environment in the powder, the heat treatment up to 100°C and the direct contact of the $(1-x)LiBH_4+xCa(BH_4)_2$ sample with the lithium electrodes facilitates the formation of both orthorhombic and cubic CaH_2 with hydrogen defects. Further research would be needed to clarify the exact mechanism for such a formation. Note that it cannot be fully excluded that trace amounts of fluoride are present in this phase, and that it is in fact a $CaH_{2-x}F_x$ solid solution with a very small fluoride concentration. However, since the only source of fluoride would in this case be a TEFLON rig in the impedance spectroscopy experimental setup, with which the sample was never in direct contact, this is considered very unlikely. It can also not be excluded that some of the detected CaH_2 is indeed $Ca_{1-x}Li_xH_{2-x}$, since the formation of the new phase takes place in close proximity with the Li electrodes. No indications of this could, however, be found in the Rietveld refinement of the diffraction pattern in Figure 2, and the formation of such a phase is not expected as LiH_2 and CaH_2 do not easily form a new compound, but rather form a eutectic mixture [69].

The two CaH_2 phases detected in the diffraction pattern in Figure 2 are expected to be a product of a reaction between some combination of $Ca(BH_4)_2$, $LiBH_4$ and/or Li. It must therefore be assumed that one or more phases containing the corresponding amount of boron are formed as well. No such phase is observed in the XRD data, and the formation of CaB_6 or some other phase containing the relatively highly scattering calcium atom is therefore not expected. As already mentioned, elemental boron would not necessarily be detectable in the diffraction pattern, and could be present although no diffraction peaks are assigned to it. Crystalline boron is black and could possibly be responsible for the black color of the layers that form at the interface between the composites and the lithium electrodes. Its formation along with the formation of CaH_2 cannot be fully excluded. It must, however, be noted that elementary boron is considered very difficult to obtain, and is generally not observed as a reaction product of thermal decomposition of borohydrides below temperatures around 250°C [70,71]. Therefore, we do not consider it very likely that the majority of the boron atoms that become available during the reaction that forms CaH_2 go into the formation of elemental boron.

It is, on the other hand, considered very likely that diborane (B_2H_6) gas is released along with the formation of CaH_2. Diborane is typically released during thermal decomposition of borohydrides below 250°C [23,72,73], but dissociates at that temperature [74]. It has proven difficult to avoid its formation in research on borohydrides for reversible hydrogen storage applications [71], and was very likely formed during this work as well. Its formation could not be observed with the experimental methods used in this work, but this could be addressed using mass spectroscopy in further studies on this topic. Although the reaction responsible for the formation of CaH_2 in this work does not necessarily involve thermal decomposition of the borohydrides, we still consider it very likely that diborane is released during the formation of CaH_2.

To gain more information on the surface composition, chemical bonds and morphology of the black-colored powder, XPS and SEM/EDS measurements were performed. The XPS results (which are included as supporting information) indicate that the only type of chemical bonds in the sample that involves calcium are Ca-H bonds. No Ca-F bonds were detected. This strongly suggests that the two CaH_2 phases are the only new calcium phases that have been formed in the sample during the heat treatment, and that no CaF_2 or amorphous phases are present. The only chemical bonds of boron detected in the XPS measurements were B-H bonds and B-O bonds. A very small signal of the latter bond type was detected, most likely originating from slight impurities in the sample. It should, however, be noted that B-B bonds have a binding energy very similar to B-H bonds, and a possible signal from boron bonds may therefore be drowned out by the signal from hydrogen bonds.

Figure 4 shows a SEM image of a black colored part of $0.875LiBH_4+0.125Ca(BH_4)_2$ powder after the heat treatment during the impedance spectroscopy measurement. An additional SEM image is included as supporting information. Elemental mapping of the microscope image was performed using the EDS technique. The bulk of the powder appears dark gray on the image and is found to have a rather constant concentration of both calcium

and boron. These areas are expected to mainly consist of a physical mixture of $LiBH_4$ and $Ca(BH_4)_2$. The powder also contains small areas that appear light gray and were found to be calcium-rich. These areas are, however, not boron-rich, excluding the possibility that they consist of $Ca(BH_4)_2$. The EDS instrument is unfortunately not capable of detecting hydrogen, which is limiting for the conclusions that can be drawn from the SEM/EDS measurements in this study. But since the XPS results only indicate the presence of Ca-H bonds and no other bonds involving calcium, it is reasonable to assume that the calcium-rich areas in the SEM image are in fact CaH_2. It is of course also possible that these areas consist of pure calcium, but after the heat treatment this is not considered very likely. Although the EDS results are not strictly conclusive on their own, they are in good agreement with the XRD and XPS data, and strengthen the hypothesis that CaH_2 is formed. With the combined results from the calculations and from the XRD, XPS and EDS measurements, we thus conclude that the two CaH_2 phases (orthorhombic and cubic) have been formed during the heat treatment.

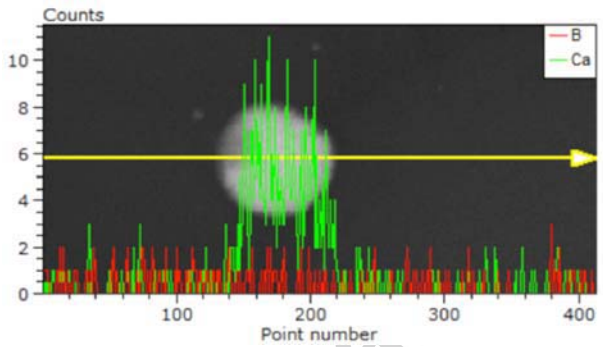

Figure 4 A SEM image of a black-colored part of a $0.875LiBH_4+0.125Ca(BH_4)_2$ sample after heat treating it up to a temperature of 100°C during the impedance spectroscopy measurements. Elemental mapping using EDS revealed that the bulk of the powder is a physical mixture of $LiBH_4$ and $Ca(BH_4)_2$, possibly along with some elemental boron, while areas that appear light gray in the microscope were found to be calcium-rich. The light gray particle in the middle of the image is approximately 10 µm in diameter. The result of an elemental mapping line scan is shown. A clear increase in calcium concentration is detected at the position of the light gray area, but no increase in the concentration of boron (or any other element) is detected. Note that the EDS equipment cannot detect hydrogen or lithium. Also note that the colors of the SEM image do not represent the actual colors of the sample, and that the light gray area in the figure may thus well be black in reality.

3.3 Conductivity

The conductivity of $(1-x)LiBH_4+xCa(BH_4)_2$ was measured for three mixing ratios, i.e. $x = \{1/4, 1/2, 3/4\}$. Figure 5 shows examples of Nyquist plots obtained by impedance spectroscopy. All Nyquist plots showed one arc (a slightly depressed semi-circle). The explanation for this can be either that only one contribution to the conduction is present, or that two or more arcs of concurrent bulk and/or grain boundary contributions overlap completely in the Nyquist plots. Unfortunately, it is not possible to separate different contributions to the conductivity in such a case using only impedance spectroscopy [75,76].At the highest temperatures, some of the Nyquist plots also showed a small tail at the low-frequency end, which is attributed to the lithium electrodes.

As the Nyquist plots only show one arc, they were fitted using an (RQ) equivalent circuit model, i.e. a resistor and a constant phase element (CPE) in parallel. The Nyquist plots containing a low-frequency tail were fitted using two such circuits in series. The sample resistance R was taken to be the point of intersection between the Z' axis and the low-frequency end of the large arc. The conductivity of the samples is given by

$$\sigma = \frac{d}{AR} \qquad (1)$$

where R is the resistance obtained from the (RQ) fit, d is the thickness of the sample and A its area.

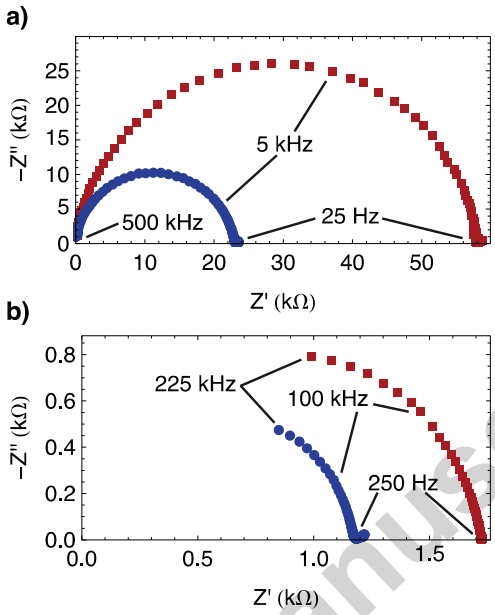

Figure 5 Examples of Nyquist plots obtained from impedance spectroscopy on $0.5LiBH_4+0.5Ca(BH_4)_2$. The red squares are measured during heating, the blue circles are measured during cooling. a) Measurements performed at 40°C. b) Measurements performed at 80°C. The Nyquist plots mostly show only one arc, but at the higher temperatures a small contribution from the electrodes is sometimes observed at the low-frequency end of the plots.

The ionic conductivities of the $(1-x)LiBH_4+xCa(BH_4)_2$ samples are shown in Figure 6. The conductivity of pure $LiBH_4$, both as-received (non-milled) and ball-milled, is shown for comparison. Attempts were made at measuring the conductivity of pure $Ca(BH_4)_2$. This did, however, not succeed, most probably due to the ionic conduction of $Ca(BH_4)_2$ being too poor for measurements with this experimental setup (i.e. $<10^{-9}$ S/cm).

The ionic conductivity of the samples is very sensitive to defects in the crystal structure of the powders. The ball-milled $LiBH_4$ has a much higher conductivity ($4.6*10^{-5}$ S/cm at 40°C) than the non-milled (as-received) sample ($2.4*10^{-8}$ S/cm at 40°C), although both samples are in the orthorhombic, poorly conducting phase. This can be explained by the formation of defects during the milling which may open new Li^+ conduction pathways[33]. As the sample is only heated up to 100°C, and not above the $LiBH_4$ phase transition temperature of approximately 110°C, the defects are not mended by the heat treatment and the conductivity of the ball-milled $LiBH_4$ remains similar during cooling.

The $(1-x)LiBH_4+xCa(BH_4)_2$ pellets consisted of as-milled powders. The $3/4LiBH_4+1/4Ca(BH_4)_2$ sample has the highest conductivity of the measured composites, or $8.8*10^{-6}$ S/cm at 40°C. A comparison of the phase compositions shown in Figure 1 with the conductivities of the composite samples shown in Figure 6 indicates that the presence of α-$Ca(BH_4)_2$ grain boundaries might be slightly more favorable for the conductivity than the presence of γ-$Ca(BH_4)_2$ grain boundaries. The ionic conductivity of all the composite samples is, however, in the range of 0.001 - 0.01 mS/cm, and thus considerably lower than the aforementioned conductivity target of 1 mS/cm. This is probably too low for application as a bulk electrolyte in working battery cells. However, at 100°C the $3/4\ LiBH_4+1/4Ca(BH_4)_2$

sample reaches a conductivity of 1 mS/cm, which might be of interest in battery applications at elevated temperatures.

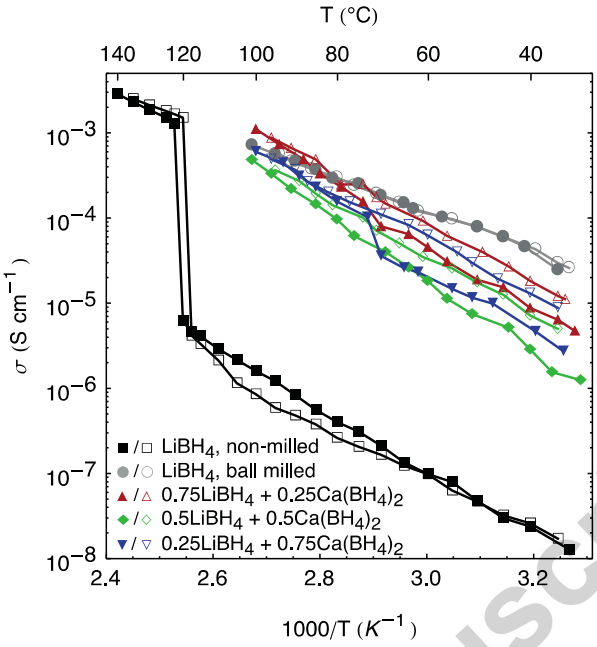

Figure 6 An Arrhenius plot of the ionic conductivity of the $LiBH_4$+$Ca(BH_4)_2$ mixtures. The ionic conductivity of non-milled and ball-milled pure $LiBH_4$ is shown for comparison. The filled symbols denote measurements during heating runs, the empty symbols denote measurements during cooling runs. The conductivity of the composites is in all cases lower than that of the ball-milled $LiBH_4$. Note that the conductivity of the composite samples is in all cases higher during cooling than during heating. This is most probably an artifact due to the formation of a defect-rich, electronically conducting CaH_2 phase at the electrode-electrolyte interfaces of the pellets, but not due to an increase in the ionic conductivity of the samples.

The fact that the Nyquist plots (see Figure 5) only show one arc that can be related to bulk and/or grain boundary conduction strongly suggests that Li^+ is the only charge carrier in the composite, i.e. that the contribution of Ca^{+2} to the conduction is negligible, This hypothesis is further strengthened by the observation that the conductivities of the (1-x)$LiBH_4$+$x$$Ca(BH_4)_2$ samples are only slightly lower than that of ball-milled pure $LiBH_4$ (see Figure 6) while the ionic conduction of pure $Ca(BH_4)_2$ is very poor.

The presence of Ca^{+2} vacancies in α-$Ca(BH_4)_2$ (which is indicated by the Rietveld refinement of the synchrotron data, see Table 1) could indicate that some Ca^{+2} substitute into $LiBH_4$, or that they form a grain boundary interface of Ca^{+2}. The formation of such an interface could enhance the ionic conduction in the $LiBH_4$-$Ca(BH_4)_2$ composite. The difference in the activation energies, which are derived from the slope of the Arrhenius plots, could also be an indication that the conduction mechanisms differ slightly between the pure $LiBH_4$ and the composites. The activation energy of the ball-milled $LiBH_4$ is found to be around 0.55 eV while the activation energies of the composites are found to be approximately 0.8 eV in all cases. Further work using other experimental techniques would be needed to determine which conductive species contribute to the ionic conductivity of the (1-x)$LiBH_4$+$x$$Ca(BH_4)_2$ composite.

In the impedance spectroscopy measurements, the conductivity of the composites is in all cases found to be higher during cooling runs (see Figure 6), i.e. after the samples have been heated to 100°C in the impedance spectroscopy setup and the black powder discussed in section 3.2 has formed. If one or both of the CaH_2 phases were electronically conducting, so that the resistivity of the layers in which they form were negligible compared to the resistivity of the (1-x)$LiBH_4$+$x$$Ca(BH_4)_2$ composites, the contribution of the CaH_2 containing layers

would not be visible in the impedance spectroscopy measurements. This also holds true if elemental boron is formed, as boron has an electronic conductivity of 0.1 mS/cm at room temperature, which is almost 2 orders of magnitude higher than the composite samples. Furthermore, since the thickness of the pelletized samples is used to estimate the conductivity of the composites (see Eq. 1), the formation of such electronically conducting layers would result in a reduction of the effective thickness of the sample that can be related to the ionic conduction. Consequently, the measured pellet thickness d would no longer have the right value for eq. 1 and the ionic conductivity σ would be overestimated. With a continuing formation of such electronically conducting layers in the electrolyte, the pellet would eventually short circuit.

To investigate if this could be the case, and if the increased conductivity of the black layer could originate from the formation of CaH_2, the density of electronic states for the two CaH_2 phases were calculated. The density of electronic states of cubic CaH_2, as obtained from calculations with the PBE exchange correlation functional, is shown in Figure 7. In the case of cubic CaH_2, the calculations were performed with no crystal defects and with a 1/8 density of hydrogen vacancies. The band gap of orthorhombic CaH_2 was calculated to be 5.84 eV, which is in good agreement with published experimental work [77]. The band gap of defect-free, cubic CaH_2 was calculated to be 2.26 eV, which makes it a semi-conductor. This value is also not far off the result of Weaver et al. [77] who calculated the band structure of a 'hypothetical' CaH_2 phase with a cubic CaF_2 structure but a slightly smaller lattice parameter. Furthermore, cubic CaH_2 with 1/8 density of hydrogen vacancies has electronic states that reach below the Fermi level and is therefore electronically conducting, according to the calculations. This is the case both for charged (shown in Figure 7) and charge neutral vacancies. This could explain the increase in conduction of the samples that takes place upon the formation of CaH_2. Calculations of the band gap of cubic $CaH_{2-x}F_x$ in various mixing ratios are included as supporting information.

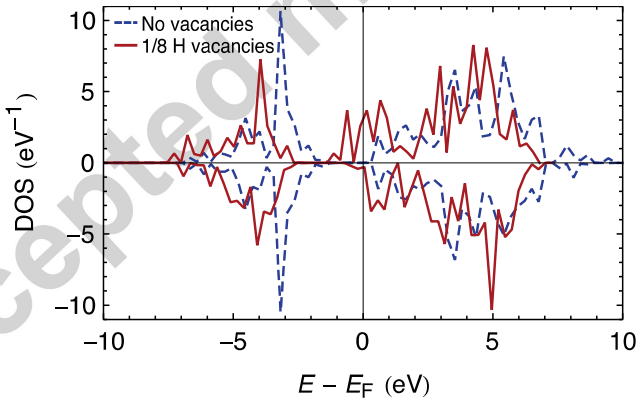

Figure 7 The calculated density of states of CaH_2 in the cubic CaF_2 crystal structure. E_F denotes the Fermi energy of the system. The results are shown for a structure without vacancies (blue, dashed lines), and for a structure with 1/8 density of negatively charged hydrogen vacancies (red, solid lines). In the structure containing vacancies, there are states that extend below the Fermi level, which suggests that the phase is electronically conducting.

The total thickness of the two black layers in each pellet was, in most cases, estimated to be around 50% of the pellet's total thickness. Assuming that these layers are electronically conducting (with an electronic conduction that is much higher than the ionic conduction of the samples), one would expect the measured conductivity to double compared to the original pellet. A comparison of the conductivity values of the composite samples near room temperature before and after the heat treatment shows that this estimate is not far off. As an example, the conductivity of $0.75LiBH_4+0.25Ca(BH_4)_2$ at 35°C is measured at $6.4*10^{-6}$ S/cm before the heat treatment and $1.21*10^{-5}$ S/cm after the heat treatment, which is an increase by

a factor of 1.9. If a thicker conducting layer were to be formed in the cell, or if the cells had a thinner layer of electrolyte to begin with, this effect would pose a serious risk of an internal short circuit in the cell.

The conclusion is therefore, that the measured conductivity after the heat treatment is always higher than prior to the heat treatment because of the unwanted formation of electronically conducting cubic CaH_2 with hydrogen defects near the lithium electrodes of the pelletized samples, along with the possible formation of elemental boron. Further research is needed and to clarify if elemental boron is formed or not and if its possible presence also contributes to the increased conductivity of the samples. This artifact, which arises due to a low chemical stability of the composites, poses a serious risk that the pelletized samples would eventually short-circuit with continued formation of the conducting layer. This observation is not encouraging for the idea of developing working battery cells containing the composite, but could nonetheless be of fundamental scientific interest. This finding furthermore highlights a serious general issue, namely that a slow formation of an electronically conducting layer in any solid electrolyte might eventually lead to a short-circuit. The chemical stability of any potential solid electrolyte material must therefore be investigated thoroughly before its introduction in commercial battery cells.

4. Summary and Outlook

The $(1\text{-}x)LiBH_4+xCa(BH_4)_2$ composite forms a physical mixture of three phases, as measured with synchrotron x-ray diffraction; α-$Ca(BH_4)_2$, γ-$Ca(BH_4)_2$ and orthorhombic $LiBH_4$. The formation of a solid solution is not observed. Rietveld refinement of the diffraction patterns reveals that the relative fractions of the two $Ca(BH_4)_2$ phases changes considerably with $LiBH_4$ content, and γ-$Ca(BH_4)_2$ is found to be the dominant phase for $x \geq 0.5$. No β-$Ca(BH_4)_2$ is observed in the composite samples, although a third of the precursor $Ca(BH_4)_2$ powder had that crystal structure. Instead, a considerable fraction of the powder takes on the α-$Ca(BH_4)_2$ structure when small amounts $LiBH_4$ are added.

The formation of small amounts of two different phases of CaH_2 is observed upon heat treatment up to 100°C during the impedance spectroscopy measurements. These are CaH_2 in its regular orthorhombic (*Pnma*) crystal structure and CaH_2 in a cubic (*Fm-3m*) CaF_2-type crystals structure. This result from the Rietveld refinement of synchrotron x-ray data is further supported by XPS and SEM/EDS data. The possibility of the formation of elemental boron is not excluded, and further research is needed to clarify that. The relative stability of CaH_2 was calculated for both phases. The results indicate that cubic and orthorhombic CaH_2 with a 1/8 density of hydrogen defects are approximately equally stable, supporting the observed coexistence of the two phases.

As no hexagonal $LiBH_4$ was observed in the composites, the ionic conductivity of $(1\text{-}x)LiBH_4+xCa(BH_4)_2$ is not as high as for example that of the $LiBH_4$+LiI solid solution [24]. Defects induced by ball milling do, however, increase the ionic conduction of orthorhombic $LiBH_4$ considerably ($4.6*10^{-5}$ S/cm at 40°C). The ionic conduction of $(1\text{-}x)LiBH_4+xCa(BH_4)_2$ is, for all measured values of x, lower than that of the ball-milled $LiBH_4$. The $0.75LiBH_4+0.25Ca(BH_4)_2$ mixture has the best conductivity of the composites; $8.8*10^{-6}$ S/cm at 40°C and 1 mS/cm at 100°C. Near room temperature, this is considerably lower than the conductivity target of 1 mS/cm, which is often mentioned as the minimum conductivity required for an electrolyte in a consumer battery. The composite, might, however, be of potential interest for battery applications at elevated temperatures.

It is not clear if lithium ions are the only charge carrier in the composites, or if calcium ions also participate in the conduction. The single-arc Nyquist plots and the slightly lower conductivity than ball-milled $LiBH_4$ suggest that Li^+ is the only charge carrier. However, the difference in the activation energy of the conduction between $LiBH_4$ and the composites indicates that the systems do not share the exact same conduction mechanism. Further work would be needed to clarify this.

The results of electronic band structure calculations for orthorhombic and cubic CaH_2, with and without hydrogen defects, indicate that the cubic structure with defects is

electronically conducting. Elemental boron, if present, is also electronically conducting. This most probably explains the high conductivity observed for the heat-treated composites. The formation of an electronically conducting layer within the electrolyte in the cells is an unwanted artifact in the conductivity measurements, which increases the risk of short-circuiting in the cells. This finding reveals a more general issue that could be detrimental to other solid electrolytes and is thus of interest for further studies.

Associated Content

Supporting information

XPS data, additional SEM data and additional band gap calculations are available as supporting information.

Author Information

Corresponding author

Tejs Vegge, phone: +45 46775810; fax: +45 46775688; e-mail: teve@dtu.dk.

Author Contributions

The manuscript was written through contributions of all authors. All authors have given approval to the final version of the manuscript. The authors declare no competing financial interest.

Acknowledgements

The authors would like to acknowledge support from the Danish Ministry of Science Globalization Fund, the European Graduate School on Sustainable Energy – The Molecular Approach, the Danish Center for Scientific Computing, the Danish Council for Strategic Research (the ReLiable project), the Diamond Light Source in Oxfordshire, UK, the Swiss-Norwegian Beam Lines at ESRF in Grenoble, France and the Catalysis for Sustainable Energy (CASE) initiative. CASE is funded by the Danish Ministry of Science, Technology, and Innovation.

References

[1] J.-M. Tarascon, M. Armand, Issues and Challenges Facing Rechargeable Lithium Batteries., Nature. 414 (2001) 359–67.

[2] P. Knauth, Inorganic Solid Li ion Conductors: An Overview, Solid State Ionics. 180 (2009) 911–916.

[3] J.B. Goodenough, Y. Kim, Challenges for Rechargeable Li Batteries, Chem. Mater. 22 (2010) 587–603.

[4] J.-M. Tarascon, Key Challenges in Future Li-Battery Research., Phil. Trans. R. Soc. A. 368 (2010) 3227–41.

[5] A. Rabenau, Lithium Nitride and Related Materials, Case Study of The Use of Modern Solid State Research Techniques, Solid State Ionics. 6 (1982) 277–293.

[6] A.G. Belous, G.N. Novitskaya, S. V. Polyanetskaya, Y.I. Gornikov, No Title, Izv. Akad. Nauk SSSR. 23 (1987) 470–472.

[7] Y. Inaguma, C. Liquan, M. Itoh, T. Nakamura, T. Uchida, H. Ikuta, et al., High Ionic Conductivity in Lithium Lanthanum Titanate, Solid State Commun. 86 (1993) 689–693.

[8] O. Bohnke, The Fast Lithium-Ion Conducting Oxides Li3xLa2/3−xTiO3 From Fundamentals to Application, Solid State Ionics. 179 (2008) 9–15.

[9] V. Thangadurai, J. Schwenzel, W. Weppner, Tailoring Ceramics for Specific Applications: A Case Study of the Development of All-Solid-State Lithium Batteries, Ionics (Kiel). 11 (2005).

[10] H. Aono, E. Sugimoto, Y. Sadaoka, N. Imanaka, G. Adachi, Electrical Property and Sinterability of LiTi2 (PO4)3 Mixed With Lithium Salt (Li3PO4 or Li3BO3), Solid State Ionics. 47 (1991) 257–264.

[11] K. Arbi, J.M. Rojo, J. Sanz, Lithium Mobility in Titanium Based Nasicon Li1+xTi2−xAlx(PO4)3 and LiTi2−x Zrx(PO4)3 Materials Followed by NMR and Impedance Spectroscopy, J. Eur. Ceram. Soc. 27 (2007) 4215–4218.

[12] P.G. Bruce, A.R. West, The A-C Conductivity of Polycrystalline LISICON, Li2+Zn, xGeO4, and a Model for Intergranular Constriction Resistances, J. Electrochem. Soc. 130 (1983) 662–669.

[13] N. Kamaya, K. Homma, Y. Yamakawa, M. Hirayama, R. Kanno, M. Yonemura, et al., A Lithium Superionic Conductor, Nat. Mater. 10 (2011) 682–686.

[14] S. Stramare, V. Thangadurai, W. Weppner, Lithium Lanthanum Titanates: A Review, Chem. Mater. 15 (2003) 3974–3990.

[15] R.J. Brodd, W. Huang, J.R. Akridge, Polymer Battery R&D in the U.S., Macromol. Symp. 159 (2000) 229–245.

[16] M. Park, X. Zhang, M. Chung, G.B. Less, A.M. Sastry, A Review of Conduction Phenomena in Li-Ion Batteries, J. Power Sources. 195 (2010) 7904–7929.

[17] J.Y. Song, Y.Y. Wang, C.C. Wan, Conductivity Study of Porous Plasticized Polymer Electrolytes Based on Poly(vinylidene fluoride) A Comparison with Polypropylene Separators, J. Electrochem. Soc. 147 (2000) 3219–3225.

[18] A. Züttel, S. Rentsch, P. Fischer, P. Wenger, P. Sudan, P. Mauron, et al., Hydrogen Storage Properties of LiBH4, J. Alloy. Comp. 356-357 (2003) 515–520.

[19] Z. Łodziana, T. Vegge, Structural Stability of Complex Hydrides: LiBH4 Revisited, Phys. Rev. Lett. 93 (2004) 145501.

[20] J.K. Kang, S.Y. Kim, Y.S. Han, R.P. Muller, W. a. Goddard, A candidate LiBH4 for Hydrogen Storage: Crystal Structures and Reaction Mechanisms of Intermediate Phases, Appl. Phys. Lett. 87 (2005) 111904.

[21] Z. Łodziana, T. Vegge, Structural Stability of Complex Hydrides: LiBH4 Revisited Comment: Łodziana and Vegge Reply, Phys. Rev. Lett. 97 (2006) 119602.

[22] L. Mosegaard, B. Møller, J.-E. Jørgensen, U. Bösenberg, M. Dornheim, J.C. Hanson, et al., Intermediate Phases Observed During Decomposition of LiBH4, J. Alloy. Comp. 446-447 (2007) 301–305.

[23] D. Blanchard, Q. Shi, C.B. Boothroyd, T. Vegge, Reversibility of Al/Ti Modified LiBH4, J. Phys. Chem. C. 113 (2009) 14059–14066.

[24] M. Matsuo, Y. Nakamori, S. Orimo, H. Maekawa, H. Takamura, Lithium Superionic Conduction in Lithium Borohydride Accompanied by Structural Transition, Appl. Phys. Lett. 91 (2007) 224103.

[25] V. Epp, M. Wilkening, Fast Li Diffusion in Crystalline LiBH4 Due to Reduced Dimensionality: Frequency-Dependent NMR Spectroscopy, Phys. Rev. B. 82 (2010) 020301.

[26] T. Ikeshoji, E. Tsuchida, T. Morishita, K. Ikeda, M. Matsuo, Y. Kawazoe, et al., Fast-Ionic Conductivity of Li+ in LiBH4, Phys. Rev. B. 83 (2011) 144301.

[27] M. Matsuo, S. Orimo, Lithium Fast-Ionic Conduction in Complex Hydrides: Review and Prospects, Adv. En. Mat. 1 (2011) 161–172.

[28] J.-P. Soulié, G. Renaudin, R. Černý, Y. K, Lithium Boro-Hydride LiBH 4 I. Crystal Structure, J. Alloy. Comp. 346 (2002) 200–205.

[29] H. Maekawa, M. Matsuo, H. Takamura, M. Ando, Y. Noda, T. Karahashi, et al., Halide-Stabilized LiBH4, a Room-Temperature Lithium Fast-Ion Conductor., J. Am. Chem. Soc. 131 (2009) 894–895.

[30] H. Oguchi, M. Matsuo, J.S. Hummelshøj, T. Vegge, J.K. Nørskov, T. Sato, et al., Experimental and Computational Studies on Structural Transitions in the LiBH4–LiI Pseudobinary System, Appl. Phys. Lett. 94 (2009) 141912.

[31] R. Miyazaki, T. Karahashi, N. Kumatani, Y. Noda, M. Ando, H. Takamura, et al., Room Temperature Lithium Fast-Ion Conduction and Phase Relationship of LiI Stabilized LiBH4, Solid State Ionics. 192 (2011) 143–147.

[32] L.H. Rude, E. Groppo, L.M. Arnbjerg, D.B. Ravnsbæk, R. a. Malmkjær, Y. Filinchuk, et al., Iodide Substitution in Lithium Borohydride, LiBH4–LiI, J. Alloy. Comp. 509 (2011) 8299–8305.

[33] D. Sveinbjörnsson, J.S.G. Myrdal, D. Blanchard, J.J. Bentzen, T. Hirata, M.B. Mogensen, et al., Effect of Heat Treatment on the Lithium Ion Conduction of the LiBH4−LiI Solid Solution, J. Phys. Chem. C. 117 (2013) 3249–3257.

[34] J.S.G. Myrdal, D. Blanchard, D. Sveinbjörnsson, T. Vegge, Li-ion Conduction in the LiBH 4 : LiI System from Density Functional Theory Calculations and Quasi-Elastic Neutron Scattering, J. Phys. Chem. C. 117 (2013) 9084–9091.

[35] K. Miwa, M. Aoki, T. Noritake, N. Ohba, Y. Nakamori, S. Towata, et al., Thermodynamical stability of calcium borohydride Ca(BH4)2, Phys Rev. B. 74 (2006) 1–5.

[36] E. Rönnebro, E.H. Majzoub, Calcium borohydride for hydrogen storage: catalysis and reversibility., J. Phys. Chem B. 111 (2007) 12045–7.

[37] M.D. Riktor, M.H. Sørby, K. Chłopek, M. Fichtner, F. Buchter, A. Züttel, et al., In situ synchrotron diffraction studies of phase transitions and thermal decomposition of Mg(BH4)2 and Ca(BH4)2, J. Mater. Chem. 17 (2007) 49394942.

[38] J.-H. Kim, S.-A. Jin, J.-H. Shim, Y.W. Cho, Thermal decomposition behavior of calcium borohydride Ca(BH4)2, J. Alloy. Comp. 461 (2008) L20–L22.

[39] M. Aoki, K. Miwa, T. Noritake, N. Ohba, M. Matsumoto, H.W. Li, et al., Structural and dehydriding properties of Ca(BH4)2, Appl. Phys. A. 92 (2008) 601–605.

[40] M.D. Riktor, M.H. Sørby, K. Chłopek, M. Fichtner, B.C. Hauback, The identification of a hitherto unknown intermediate phase CaB2Hx from decomposition of Ca(BH4)2, J. Mater. Chem. 19 (2009) 2754–2759.

[41] D. Blanchard, M.D. Riktor, J.B. Maronsson, H.S. Jacobsen, J. Kehres, D. Sveinbjörnsson, et al., Hydrogen Rotational and Translational Diffusion in Calcium Borohydride from Quasielastic Neutron Scattering and DFT Calculations, J. Phys. Chem. C. 114 (2010) 20249–20257.

[42] I. Llamas-Jansa, O. Friedrichs, M. Fichtner, E.G. Bardaji, A. Züttel, B.C. Hauback, The Role of Ca(BH 4) 2 Polymorphs, J. Phys. Chem C. 116 (2012) 13472–13479.

[43] Y. Filinchuk, E. Ronnebro, D. Chandra, Crystal structures and phase transformations in Ca(BH4)2, Acta Mater. 57 (2009) 732–738.

[44] F. Buchter, Z. Łodziana, A. Remhof, O. Friedrichs, A. Borgschulte, P. Mauron, et al., Structure of Ca(BD4)2 beta-phase from combined neutron and synchrotron X-ray powder diffraction data and density functional calculations., J. Phys. Chem. B. 112 (2008) 8042–8048.

[45] F. Buchter, Z. Łodziana, A. Remhof, O. Friedrichs, A. Borgschulte, P. Mauron, et al., Structure of the Orthorhombic γ-Phase and Phase Transitions of Ca(BD4)2, J. Phys. Chem. C. 113 (2009) 17223–17230.

[46] A. Borgschulte, R. Gremaud, A. Züttel, P. Martelli, A. Remhof, A. Ramirez-Cuesta, et al., Experimental evidence of librational vibrations determining the stability of calcium borohydride, Phys. Rev. B. 83 (2011) 024102.

[47] R. Kanno, Y. Takeda, O. Yamamoto, Ionic Conductivity of Solid Lithium Ion Conductors With the Spinel Structure: Li_2MCl_4 (M = Mg, Mn, Fe, Cd), Mat. Res. Bull. 16 (1981) 999–1005.

[48] J.Y. Lee, D. Ravnsbæk, Y. Lee, Y. Kim, Y. Cerenius, J. Shim, et al., Decomposition Reactions and Reversibility of the LiBH 4 -Ca (BH 4) 2 Composite, J. Phys. Chem. C. 113 (2009) 15080–15086.

[49] Z. Fang, X. Kang, J. Luo, P. Wang, H. Li, S. Orimo, Formation and Hydrogen Storage Properties of Dual-Cation (Li , Ca) Borohydride, J. Phys. Chem. C. 114 (2010) 22736–22741.

[50] V.A. Dyadkin, SNBL Tool Box, Swiss-Norwegian Beam Lines at ESRF, Grenoble, France, 2012.

[51] A.P. Hammersley, S.O. Sveinson, M. Hanfland, A.N. Fitch, D. Hausermann, Two-dimensional Detector Software: From Real Detector to Idealised Image or Two-Theta Scan, High Pr. Res. 14 (1996) 235–248.

[52] A.C. Larson, R.B. von Dreele, Report LAUR 86-784, General Structure Analysis System (GSAS), 1994.

[53] P. Hohenberg, W. Kohn, Inhomogeneous Electron Gas, Phys. Rev. 136 (1964) 864–871.

[54] W. Kohn, L.J. Sham, Self-Consistent Equations Including Exchange and Correlation Effects, Phys. Rev. 140 (1965) 1133–1138.

[55] J. Mortensen, L. Hansen, K. Jacobsen, Real-space grid implementation of the projector augmented wave method, Phys. Rev. B. 71 (2005) 035109.

[56] J. Enkovaara, C. Rostgaard, J.J. Mortensen, J. Chen, M. Dułak, L. Ferrighi, et al., Electronic structure calculations with GPAW: a real-space implementation of the projector augmented-wave method., J. Phys. Condens. Matter. 22 (2010) 253202.

[57] S.R. Bahn, K.W. Jacobsen, An Object-Oriented Scripting Interface to a Legacy Electronic Structure Code, Comp. Sci. Eng. 4 (2002) 56–66.

[58] P.E. Blöchl, Projector Augmented-Wave Method, Phys. Rev. B. 50 (1994) 17953.

[59] P.E. Blöchl, C.J. Först, J. Schimpl, Projector Augmented Wave Method: Ab Initio Molecular Dynamics With Full Wave Functions, Bull. Mater. Sci. 26 (2003) 33.

[60] J.J. Perdew, K. Burke, M. Ernzerhof, Generalized Gradient Approximation Made Simple, Phys. Rev. Lett. 77 (1996) 3865.

[61] M. Kuisma, J. Ojanen, J. Enkovaara, T.T. Rantala, Kohn-Sham potential with discontinuity for band gap materials, Phys. Rev. B. 82 (2010) 115106.

[62] I.E. Castelli, T. Olsen, S. Datta, D.D. Landis, S. Dahl, K.S. Thygesen, et al., Computational screening of perovskite metal oxides for optimal solar light capture, Energy Environ. Sci. 5 (2012) 5814–5819.

[63] J. Brice, A. Courtoist, J. Aubry, Preparation de la solution solide hydrurofluoree CaF(2-x)Hx (0 < x < 1,24) etude structurale par diffraction des rayons x et par diffraction des neutrons, J. Solid State Chem. 24 (1978) 381–387.

[64] J.-H. Kim, J.-H. Shim, Y.W. Cho, On the reversibility of hydrogen storage in Ti- and Nb-catalyzed Ca(BH4)2, J. Power Sources. 181 (2008) 140–143.

[65] J.Y. Lee, Y.-S. Lee, J.-Y. Suh, J.-H. Shim, Y.W. Cho, Metal halide doped metal borohydrides for hydrogen storage: The case of Ca(BH4)2–CaX2 (X=F, Cl) mixture, J. Alloy. Comp. 506 (2010) 721–727.

[66] H. Smithson, C. Marianetti, D. Morgan, A. Van der Ven, A. Predith, G. Ceder, First-principles study of the stability and electronic structure of metal hydrides, Phys. Rev. B. 66 (2002) 144107.

[67] E.R. Pinatel, L.H. Rude, M. Corno, M. Kragelund, P. Ugliengo, T.R. Jensen, et al., Thermodynamic Tuning of Calcium Hydride by Fluorine Substitution, MRS Proc. 1441 (2012) 5–16.

[68] B. Li, Y. Li, K. Yang, Q. Cui, Y. Ma, G. Zou, Raman evidence of a new high-pressure phase in calcium hydride, J. Phys. Condens. Matter. 19 (2007) 226205.

[69] C.E. Messer, J.C. Eastman, R.G. Mers, A.J. Maeland, Ternary Perovskite Phases in Systems of Lithium Hydride with Barium, Strontium and Calcium Hydrides, Inorg. Chem. 2 (1964) 776–778.

[70] G. Will, B. Kiefer, Electron Deformation Density in Rhombohedral a -Boron, Z. Anorg. Allg. Chem. 627 (2001) 2100–2104.

[71] O. Friedrichs, A. Remhof, A. Borgschulte, F. Buchter, S.I. Orimo, A. Züttel, Breaking the passivation--the road to a solvent free borohydride synthesis., Phys. Chem. Chem. Phys. 12 (2010) 10919–10922.

[72] W. Grochala, P.P. Edwards, Thermal decomposition of the non-interstitial hydrides for the storage and production of hydrogen., Chem. Rev. 104 (2004) 1283–1315.

[73] A. Züttel, A. Borgschulte, S.-I. Orimo, Tetrahydroborates as new hydrogen storage materials, Scr. Mater. 56 (2007) 823–828.

[74] M. Söderlund, P. Mäki-Arvela, K. Eränen, T. Salmi, R. Rahkola, D.Y. Murzin, Catalyst Deactivation in Diborane Decomposition, Catal. Lett. 105 (2005) 191–202.

[75] N.M. Beekmans, L. Heyne, Correlation Between Impedance, Microstructure and Composition of Calcia-Stabilized Zirconia, Electrochim. Acta. 21 (1976) 303–310.

[76] S.M. Haile, D.L. West, J. Campbell, The Role of Microstructure and Processing on the Proton Conducting Properties of Gadolinium-Doped Barium Cerate, J. Mat. Res. 13 (1998) 1576–1595.

[77] J.H. Weaver, M. Gupta, D.T. Peterson, Electronic structure and bonding in CaH2: Experiment and theory, Solid State Commun. 51 (1984) 805–808.

Table of Contents Figure

An Arrhenius plot of the ionic conductivity of the $LiBH_4$-$Ca(BH_4)_2$ composites (red, blue, green). The ionic conductivity of ball milled (gray) and non-milled (black) $LiBH_4$ is shown for comparison. The filled symbols are measured during heating runs and the empty symbols are measured during subsequent cooling runs. The conductivity of the composites is in all cases higher during cooling, most probably due to the formation of an electronically conducting layer containing defect-rich cubic CaH2. Such layer formation could eventually lead to a short circuit in the cell and reveals a general issue of chemical stability that should be attended to in the development of solid electrolyte materials.

Sample (x in mol)	*α-$Ca(BH_4)_2$ (wt%)*	*β-$Ca(BH_4)_2$ (wt%)*	*γ-$Ca(BH_4)_2$ (wt%)*	*$LiBH_4$ LT (wt%)*	*Actual $LiBH_4$ wt% in sample*	*Ca^{+2} occupancy in α-$Ca(BH_4)_2$*
0.0	0.0	0.0	0.0	100.0	100.00	N/A
0.125	24.1	0.0	3.2	72.7	68.61	0.972
0.1875	22.1	0.0	13.2	64.7	57.50	N/A
0.25	39.0	0.0	10.6	50.4	48.37	0.931
0.33	6.2	0.0	46.5	47.3	38.50	N/A
0.50	8.7	0.0	62.4	28.9	23.80	0.975
0.67	18.0	0.0	65.0	17.0	12.97	N/A
0.75	15.8	0.0	62.7	21.5	9.43	N/A
1.00	0.0	36.9	63.1	0.0	0.00	N/A

Phase	*Crystal structure*	*a* (Å)	*b* (Å)	*c* (Å)
o-LiBH4	*Pnma*	7.201	4.452	6.857
α-$Ca(BH_4)_2$	*F2ddd*	8.815	13.184	7.543
o-CaH_2	*Pnma*	5.974	3.617	6.849
c-CaH_2	*Fm-3m*	5.488	5.488	5.488

Highlights

- The $LiBH_4$-$Ca(BH_4)_2$ composite forms a physical mixture rather than a solid solution.
- The formation of defect-rich, cubic CaH_2 in a CaF_2-like structure is observed.
- A new layer containing cubic CaH_2 is conducting and may lead to a short-circuit.

Table Captions

Table 1 The relative phase quantities (in weight percentage) in the $(1\text{-}x)LiBH_4+xCa(BH_4)_2$ samples, obtained from the Rietveld refinement of the XRD data. There are large variations in the phase quantities of the α and γ phases of $Ca(BH_4)_2$ with $LiBH_4$ content, but the β phase is only present in pure $Ca(BH_4)_2$. The phase quantity of orthorhombic $LiBH_4$ is expected to equal the actual $LiBH_4$ weight percentage in each sample. This means that, for an optimal refinement, the values of the fifth column of the table are expected to approach those in the sixth column. The Rietveld refinements are, however, somewhat imperfect with regard to this, most probably due to the low scattering power of $LiBH_4$ relative to $Ca(BH_4)_2$. The rightmost column of the table shows the refined Ca^{+2} occupancies in the α-$Ca(BH_4)_2$ phase, but only for those mixtures for which synchrotron data were available. The Ca^{+2} occupancies in the β-$Ca(BH_4)_2$ and γ-$Ca(BH_4)_2$ phases were found to be 1.0 in all diffractograms.

Table 2 The crystal structures and the lattice parameters of the refined structures in Figure 2. The lattice parameters of the LiBH4 and Ca(BH4)2 phases are very similar to those in the refinements shown in Figure 1.

Figure Captions

Figure 1 Powder x-ray diffraction patterns for different ratios of $(1\text{-}x)LiBH_4+xCa(BH_4)_2$. The solid, colored lines show the measured data, the dashed, black lines show the Rietveld refinement of each measurement. The tick marks below the diffraction patterns show the locations of the Bragg reflections of α-$Ca(BH_4)_2$, β-$Ca(BH_4)_2$ γ-$Ca(BH_4)_2$ and orthorhombic $LiBH_4$. No other phases were detected in the samples. The diffraction pattern of pure $LiBH_4$ only contains orthorhombic $LiBH_4$. In the diffraction pattern of pure $Ca(BH_4)_2$, β-$Ca(BH_4)_2$ and γ-$Ca(BH_4)_2$ coexist, but no α-$Ca(BH_4)_2$ is detected. In the $(1\text{-}x)LiBH_4+xCa(BH_4)_2$ mixtures, α-$Ca(BH_4)_2$, γ-$Ca(BH_4)_2$ and orthorhombic $LiBH_4$ coexist, but no β-$Ca(BH_4)_2$ is detected. All data in the figure comes from synchrotron measurements except for the sample with $x = 0.75$

Figure 2 Synchrotron XRD data (from SNBL) and a Rietveld refinement of a black-colored part of a $0.875LiBH_4+0.125Ca(BH_4)_2$ sample after it had been heat treated up to a temperature of 100°C during the impedance spectroscopy measurements. The blue, solid line shows the measured data, the black, dashed line shows the Rietveld refinement of the data and the red, solid line on the bottom shows the difference between the measured data and the refinement. The Rietveld refinement reveals that the diffraction pattern consists of α-$Ca(BH_4)_2$, and orthorhombic $LiBH_4$, along with 3.6 wt% of orthorhombic CaH_2 and 4.2 wt% of cubic CaH_2 (in a CaF_2 crystal structure). No other phases were detected. The tick marks below the diffraction patterns show the locations of the diffraction peaks for the four phases according to the Rietveld refinement.

Figure 3 The calculated stability of cubic CaH_2 relative to orthorhombic CaH_2 for structures with no defects and for structures with a 1/8 (12.5%) density of hydrogen vacancies. The cubic structure is found to be slightly more stable than the orthorhombic structure with the introduction of the H vacancies.

Figure 4 A SEM image of a black-colored part of a $0.875LiBH_4+0.125Ca(BH_4)_2$ sample after heat treating it up to a temperature of 100°C during the impedance spectroscopy measurements. Elemental mapping using EDS revealed that the bulk of the powder is a

physical mixture of $LiBH_4$ and $Ca(BH_4)_2$, possibly along with some elemental boron, while areas that appear light gray in the microscope were found to be calcium-rich. The light gray particle in the middle of the image is approximately 10 μm in diameter. The result of an elemental mapping line scan is shown. A clear increase in calcium concentration is detected at the position of the light gray area, but no increase in the concentration of boron (or any other element) is detected. Note that the EDS equipment cannot detect hydrogen or lithium. Also note that the colors of the SEM image do not represent the actual colors of the sample, and that the light gray area in the figure may thus well be black in reality.

Figure 5 Examples of Nyquist plots obtained from impedance spectroscopy on $0.5LiBH_4+0.5Ca(BH_4)_2$. The red squares are measured during heating, the blue circles are measured during cooling. a) Measurements performed at 40°C. b) Measurements performed at 80°C. The Nyquist plots mostly show only one arc, but at the higher temperatures a small contribution from the electrodes is sometimes observed at the low-frequency end of the plots.

Figure 6 An Arrhenius plot of the ionic conductivity of the $LiBH_4+Ca(BH_4)_2$ mixtures. The ionic conductivity of non-milled and ball-milled pure $LiBH_4$ is shown for comparison. The filled symbols denote measurements during heating runs, the empty symbols denote measurements during cooling runs. The conductivity of the composites is in all cases lower than that of the ball-milled $LiBH_4$. Note that the conductivity of the composite samples is in all cases higher during cooling than during heating. This is most probably an artifact due to the formation of a defect-rich, electronically conducting CaH_2 phase at the electrode-electrolyte interfaces of the pellets, but not due to an increase in the ionic conductivity of the samples.

Figure 7 The calculated density of states of CaH_2 in the cubic CaF_2 crystal structure. E_F denotes the Fermi energy of the system. The results are shown for a structure without vacancies (blue, dashed lines), and for a structure with 1/8 density of hydrogen vacancies (red, solid lines). In the structure containing vacancies, there are states that extend below the Fermi level, which suggests that the phase is electronically conducting.